Journal of Thermal Analysis and Calorimetry, Vol. 91 (2008) 2, 517–523

KINETIC MODEL OF THE OXIDATION OF $ZrSi_2$ POWDERS

H. Geßwein[1,2*], *A. Pfrengle*[1,2], *J. R. Binder*[1] *and J. Haußelt*[1,2]

[1]Institute for Materials Research III, Forschungszentrum Karlsruhe GmbH, P.O. 3640, 76021 Karlsruhe, Germany
[2]Institute of Microsystems Engineering, University of Freiburg, Germany

The oxidation kinetics of Zr-disilicide ($ZrSi_2$) powders up to temperatures of 1550°C were studied in flowing air using non-isothermal and isothermal thermogravimetric (TG) analysis. During the oxidation process two main thermal events were detected. The first stage of the oxidation reaction leads to the formation of elemental silicon as an intermediate reaction product. Upon further temperature increase the newly formed silicon is oxidized. Completely oxidized $ZrSi_2$ samples consist of $ZrSiO_4$, amorphous and crystalline SiO_2 as well as some residual ZrO_2. The experimental TG data were analysed with a model-fitting kinetic method. The gas-solid reaction is complex and can best be fitted with a multi-step reaction scheme consisting of branching reactions based on 3D diffusion mechanisms and a fractal order reaction.

Keywords: *kinetics, thermal oxidation, thermogravimetry, zirconium disilicide*

Introduction

Several zirconium silicides with different silicon contents exist in the binary phase diagram Si–Zr [1]. These intermetallic compounds are being investigated for various high temperature applications because of their relatively low densities, high melting temperatures and good oxidation resistances at elevated temperatures. The corrosion resistance is due to the formation of a passive surface layer of SiO_2 during oxidation. According to the phase diagram, the disilicide $ZrSi_2$ is the compound with the highest silicon content among the phases in the Si–Zr system. $ZrSi_2$ crystallizes in the orthorhombic space group Cmcm and decomposes peritectically at a temperature of 1584±5°C [2]. Beside its application as a refractory compound, $ZrSi_2$ is an excellent choice as a reactive starting material for reaction bonding processes [3]. Reaction bonding techniques, such as the well known reaction bonding process of aluminium oxide (RBAO) [4], are based on the heterogeneous gas-solid reaction of a metal and a gaseous oxidant. Compared to conventional ceramic processing methods, reaction bonding offers the advantage of near net shape manufacturing. Due to the exceptionally high volume expansion during the gas-solid reaction of $ZrSi_2$ with oxygen, shrinkage-free, dense $ZrSiO_4$ ceramics with good mechanical properties can be produced [3]. However, because of the strong exothermic oxidation reaction and the associated high volume expansion, typical process problems such as sample cracking and bloating may occur. Knowledge of the intrinsic oxidation kinetics can be helpful to avoid these problems.

There are not many published reports on the oxidation behaviour of $ZrSi_2$ in powder form [5, 6] and kinetic parameters for the complex oxidation process are unavailable to the best of the authors' knowledge. In the present paper, we report of the oxidation behaviour of $ZrSi_2$ powders in flowing air at temperatures up to 1550°C. A model-fitting kinetic analysis of the non-isothermal and isothermal oxidation of $ZrSi_2$ powders is presented employing thermogravimetry. The Netzsch Thermokinetics software package is used for the non-linear regression model-fitting analysis [7]. The aim of this model-fitting kinetic approach is to find a kinetic model with minimal adjustable parameters which quantitatively describes the kinetics of the complete oxidation reaction of the disilicide particles. This formal kinetic model can then be used to predict the progress of reaction under any heating profiles. From the technical aspect this data reduction is very valuable for process control and optimization, which is an important issue regarding the fabrication of defect-free reaction bonded oxide ceramics using this intermetallic compound [3, 8].

Experimental

The investigated material is zirconium disilicide $ZrSi_2$ (H.C. Starck) in powder form. To reduce the particle size, the as-received powder was milled in a Netzsch agitator mill (LMK 4, ZrO_2 milling balls and 2-propanol

* Author for correspondence: holger.gesswein@imf.fzk.de

1388–6150/$20.00

Akadémiai Kiadó, Budapest, Hungary
Springer, Dordrecht, The Netherlands

as milling media). The milled material has a specific surface area of 5.4 m^2 g^{-1}. An average particle size of d_{50}=0.9 μm and d_{90}=2.1 μm was determined using a laser-scattering particle-size-distribution analyser (Microtrac X 100).

Simultaneous TG/DTA experiments with a heating rate of 10°C min^{-1} up to temperatures of 1450°C were conducted using a Netzsch STA 449C instrument. The atmosphere was flowing artificial air (20.5% O_2 in N_2) at a rate of 50 mL min^{-1}. Sample sizes of approximately 20 mg were contained in the manufacturer's alumina crucibles (volume: 85 μL). For phase analysis and determination of the maximum mass change after complete $ZrSi_2$ oxidation, samples were oxidized at temperatures of 600, 700, 800, 900, 1000 and 1600°C for 4 h in a box furnace (Carbolite RHF 1700). Oxidized $ZrSi_2$ samples were then characterised by means of X-ray powder diffraction using a Siemens diffractometer (Model D5005) with CuK_α radiation and a solid state detector (Bruker Sol-X). The operating conditions were 40 kV and 40 mA in the angular range 15–70° in 2θ. Crystalline phase identification based on the XRD patterns was aided by the ICDD-PDF-2 database.

For kinetic analysis, a series of experiments was conducted in a Netzsch TG/DTA thermal analyser (STA 409, flowing artificial air (20.5% O_2 in N_2) at a rate of 100 mL min^{-1}). To obtain a better weighing accuracy, larger sample masses of approximately 50 mg were filled into the manufacturer's TG/DTA alumina crucibles (volume: ~350 μL). The TG baselines were corrected by subtraction of predetermined baselines run under identical conditions except for the absence of sample. The samples were heated up to 1550°C with programmed heating rates of 1, 2.5, 5 and 10°C min^{-1} followed by an isothermal hold of 4 h to ensure almost complete oxidation. Additionally isothermal runs were performed at temperatures of 500, 600, 700 and 800°C for several hours. A constant heating rate of 20°C min^{-1} to the desired oxidation temperature was used in the isothermal runs. The experimental mass change data were transformed to conversion data by using Eq. (1):

$$\alpha(t)=\frac{m_0-m_t}{m_0-m_{end}} \quad (1)$$

where α is the general variable reaction degree, m_0 is the starting sample mass, m_t the sample mass at time t and m_{end} is the sample mass after complete oxidation. Then different kinetic models were fitted to these conversion data to extract the kinetic parameters.

Results and discussion

$ZrSi_2$ powder characterisation

Figure 1 shows a SEM micrograph of the investigated milled $ZrSi_2$ powders. The particles have an irregular morphology with sizes ranging between 1 and 3 μm, which is in reasonable agreement with the laser diffractometry measurements. Assuming spherical particles, the relation $d_{BET}=6/\rho S_{BET}$, where ρ is the theoretical density of $ZrSi_2$ (ρ=4.88 g cm^{-3}) and S_{BET} is the BET surface area, holds. From the BET surface area an average grain diameter d_{BET} of 0.2 μm can be calculated. This is an effective particle size, describing the reactivity of the powder. The small value results from the fractured surfaces of the brittle intermetallic particles. The theoretical mass gain during complete $ZrSi_2$ oxidation assuming following equation:

$$ZrSi_2+3O_2\rightarrow ZrO_2+2SiO_2 \quad (2)$$

is 65.1 mass%. The experimentally determined maximum mass gain after complete oxidation of the milled powder in a box furnace at 1600°C for 4 h is approximately 60.9 mass%, indicating a pre-oxidation of the disilicide during powder synthesis and milling. The XRD pattern of the milled powder in Fig. 2 shows reflections of $ZrSi_2$ only and some very weak reflections of ZrSi and Si as impurities. From

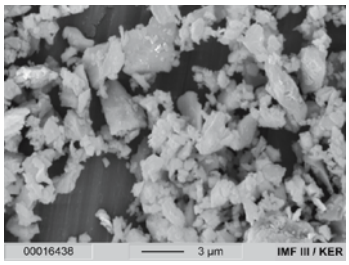

Fig. 1 SEM micrograph of agitator milled $ZrSi_2$ powder

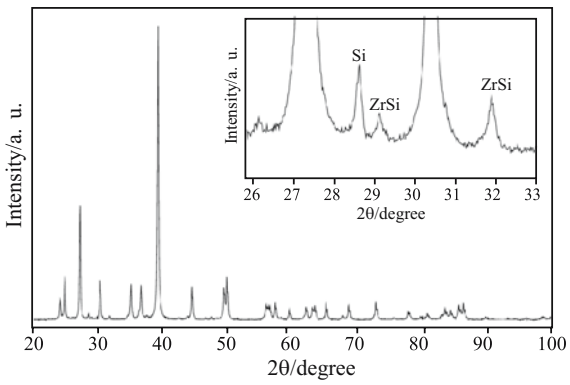

Fig. 2 XRD pattern of milled $ZrSi_2$ powder. All peaks correspond to the orthorhombic $ZrSi_2$ phase. The inset shows additional very weak reflexes of impurities of ZrSi and Si

Rietveld refinement of the diffraction pattern the mass fractions of ZrSi and Si are estimated to be 3 and 2 mass%, respectively. Other impurity phases as well as the presence of oxidized surface layers of the powder particles, which may have been formed during milling, were not detected by XRD.

Oxidation products

Oxidation products were determined from powder X-ray diffraction profiles. Figure 3 displays X-ray diffraction patterns of $ZrSi_2$ powders oxidized at 600, 700, 800, 900 and 1000°C for 4 h in a box furnace. To emphasize the low intensity diffraction peaks and the high background, a logarithmic scale for the intensity is used. The X-ray patterns of samples exposed at temperatures of 600 and 700°C show intense diffraction peaks of unreacted $ZrSi_2$, as well as the presence of monoclinic and tetragonal ZrO_2. The intensity of the strongest (131) reflex of $ZrSi_2$ at 39.1° 2θ decreases continuously with increasing oxidation temperature. At a temperature of 1000°C almost all $ZrSi_2$ is oxidized. This diffraction pattern mainly consists of broad peaks of monoclinic and tetragonal ZrO_2. The high background in the XRD patterns suggests the presence of amorphous oxidation products. The broad 'halo' in the different patterns located between 15 and 30° 2θ is shifted to smaller scattering angles with increasing oxidation temperatures indicating a change in the composition and stoichiometry of the amorphous phase. At lower oxidation temperatures the 'halo' is located at about 30° 2θ, indicating an amorphous ZrO_2 phase, whereas at higher temperatures more amorphous SiO_2 is formed and the 'halo' is located at approximately 20° 2θ. During the oxidation process elemental Si is formed as an intermediate product. The progress of the intensity of the (220) peak of Si at different oxidation temperatures is shown in Fig. 4. As can be seen, the amount of Si increases up to a temperature of 800°C, whereas at higher oxidation temperatures the intensity of the (220) peak decreases continuously due to the oxidation of the newly formed Si to amorphous SiO_x. $ZrSi_2$ samples completely oxidized at 1600°C for 4 h consist of $ZrSiO_4$, amorphous and crystalline SiO_2 as well as some residual ZrO_2.

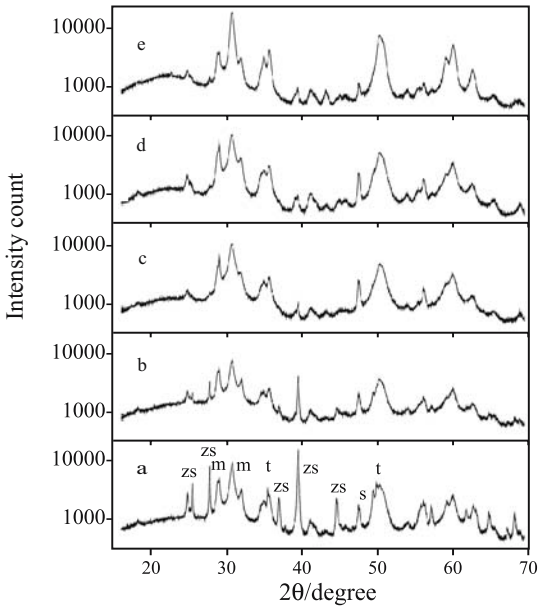

Fig. 3 XRD patterns of $ZrSi_2$ powder oxidized at a – 600°C, b – 700°C, c – 800°C, d – 900°C and e – 1000°C for 4 h under flowing air in a box furnace (ZS: $ZrSi_2$, S: Si, t: t-ZrO_2, m: m-ZrO_2)

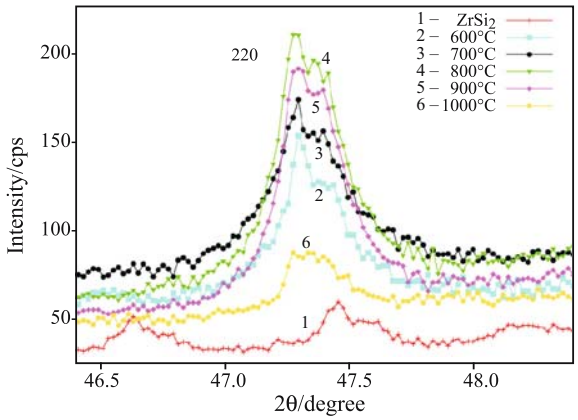

Fig. 4 Progress of the intensity of the (220) peak of Si for samples oxidized at different temperatures

The XRD results demonstrate that $ZrSi_2$ is oxidized according to the Wagner theory of selective oxidation [10–12] in which the less noble constituent of an alloy is selectively or preferentially oxidized. In the Si–Zr system silicon is more noble than zirconium and therefore silicon escapes oxidation by diffusing from the oxide layer into the bulk of the compound. Zirconium, as the less noble metal, is selectively oxidized forming an outer oxide layer. $ZrSi_2$ is the compound with the highest silicon content in the Sr–Zr system and therefore the selective oxidation results in the formation of elemental Si.

Simultaneous TG/DTA

The typical thermal profile of the oxidation of $ZrSi_2$ powder, obtained by simultaneous TG/DTA in flowing air, is presented in Fig. 5. The shape of the DTG curve corresponds to the DTA curve, which shows that the mass gain rate can be attributed to the observed exothermic effects. In general, two main thermal events can be clearly distinguished. Oxidation starts at a temperature of approximately 500°C and the sample mass increases continuously up to 900°C. The associated DTA and DTG peak maxima are located at approxi-

Table 1 $f(\alpha)$ functions for the most common mechanisms in heterogeneous kinetics

Model	Symbol	$f(\alpha)$
One-dimensional diffusion	D1	$1/2\alpha$
Two-dimensional diffusion	D2	$-(1/\ln(1-\alpha))$
Three-dimensional diffusion (Jander)	D3	$3(1-\alpha)^{2/3}/2[1-(1-\alpha)^{1/3}]$
Three-dimensional diffusion (Ginstling-Brounshtein)	D4	$3/2[(1-\alpha)^{-1/3}-1]$
Three-dimensional diffusion (exact solution of Fick's law)	D3F	see appendix
n^{th} order	Fn	$(1-\alpha)^n$
Phase boundary controlled	Rn($1\leq n\leq 3$)	$n(1-\alpha)^{1-1/n}$
Nucleation and growth (Avrami-Erofeev)	An($0.5\leq n\leq 4$)	$n(1-\alpha)[-\ln(1-\alpha)]^{1-1/n}$

Table 2 Kinetic results derived from non-linear regression for the best fitting two-step model based on two consecutive reactions (A→B→C). For the definition of the kinetic parameters see [9]

	Reaction type	Parameter	Value	Correlation-coefficient
d:f	D3F	$\log(A_1/s^{-1})$	4.437±0.152	0.99812
		E_{a1} / kJ mol^{-1}	179±3	
	D3F	$\log(A_2/s^{-1})$	1.087±0.289	
		E_{a2} /kJ mol^{-1}	168±8	
		FollReact1	0.76±0.01	

d:f: two consecutive steps, FollReact1: share of step 1 in the total mass increase

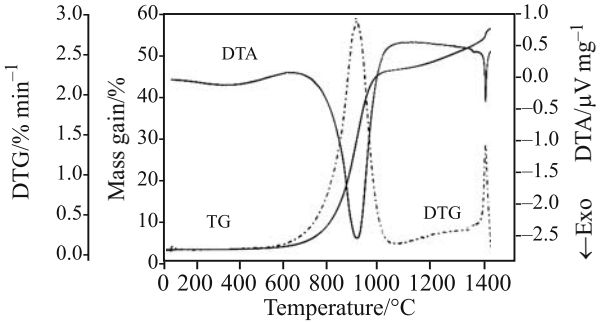

Fig. 5 DTA-TG-DTG curves recorded during heating of milled $ZrSi_2$ powder up to 1450°C at a rate of 10°C min^{-1} in flowing air (sample mass ~20 mg, thermal analyser: STA 449°C)

mately 840°C. This first part of the oxidation process has a mass gain of approximately 45%. With increasing temperature a second oxidation process with a mass change of approximately 14% and a much lower mass gain rate compared to the first step can be observed. According to the XRD results the first oxidation step can be associated with the selective oxidation of $ZrSi_2$ to ZrO_2, SiO_x and elemental Si. The observed mass change of approximately 45% is slightly higher than the theoretical value of 43.3% for the oxidation reaction represented by Eq. (3a):

$$ZrSi_2 \rightarrow ZrO_2+SiO_2+Si \quad (3a)$$

The second oxidation step which is observed at higher temperatures can be attributed to the oxidation of elemental Si, which has been formed during the selective oxidation reaction. This oxidation step can be represented by Eq. (3b):

$$ZrO_2+SiO_2+Si \rightarrow ZrO_2+2SiO_2 \quad (3b)$$

and is associated with a theoretical mass change of 15.2%. The sharp DTA/DTG peak at 1420°C and the corresponding small mass increase indicate an increased reactivity of the almost completely oxidized disilicide particles. This is most likely due to the cracking of the protective oxide layer, resulting from the formation of $ZrSiO_4$ from the newly formed SiO_2 and ZrO_2.

From the XRD and TG/DTA results it is evident that the reaction mechanism of the gas-solid oxidation of the $ZrSi_2$ particles is complex and changes during the course of reaction. Thus, it seems unlikely that this complex overall reaction can be described with a simple single-step reactin. Therefore, a multi-step

Table 3 Kinetic results derived from non-linear regression for the best fitting three-step model. For the definition of the kinetic parameters see [9]

	Reaction type	Parameter	Value	Correlation-coefficient
t:*c*,*p*	D3F	$\log(A_1/s^{-1})$	0.768±0.515	0.99948
		E_{a1}/kJ mol^{-1}	125±9	
	D3F	$\log(A_2/s^{-1})$	8.363±0.240	
		E_{a2}/kJ mol^{-1}	257±5	
	Fn	$\log(A_3/s^{-1})$	2.928±0.207	
		E_{a3}/kJ mol^{-1}	170±5	
		n	2.3±0.1	
		FollReact2	0.733±0.007	

t:*c*,*p*: three-step model, consisting of concurrent and parallel reactions
FollReact2: share of reaction pathway 2 in the total mass increase

model-fitting approach is used to describe the reaction kinetics. This is discussed in the next paragraph. Such a model-fitting approach was also successfully applied to describe the oxidation kinetics of the intermetallic compound $ZrAl_3$ [13] as well as the oxidation kinetics of magnetite using simultaneous TG/DSC data [14].

Oxidation kinetics

In thermal analysis the kinetics of solid-state reactions are generally described in terms of a 'kinetic triplet' E, A and $f(\alpha)$ according to the following equation:

$$\frac{d\alpha}{dt}=k(T)f(\alpha)=A\exp\left(-\frac{E_a}{RT}\right)f(\alpha) \qquad (4)$$

where α is the conversion degree, in thermogravimetric studies defined as in Eq. (1), t the time, T the temperature, $k(T)$ the rate constant, A the pre-exponential factor, E_a the apparent activation energy and R is the gas constant. For non-isothermal data obtained at a constant heating rate $\beta=dT/dt$, $d\alpha/dt$ in Eq. 4 is replaced with $\beta\, d\alpha/dT$. The above equation may be extended to describe complex processes such as concurrent or consecutive reactions, each with its own kinetic triplet. The reaction models $f(\alpha)$, most commonly used in heterogeneous kinetics, are listed in Table 1. The full data sets which serve as input to the kinetics software are presented in Fig. 6.

Because it has been established in the previous sections, that elemental Si is formed as an intermediate phase in the oxidation $ZrSi_2$ and because of the complex multistage process, visible in the TG curves, attempts were made to fit a range of multi-step processes to the thermogravimetric data. A model-free isoconversion method (the results from this analysis are not included in this paper) was used for an initial estimate of the kinetic parameters. These values were then used as starting parameters for the non-linear regression model-fitting procedure.

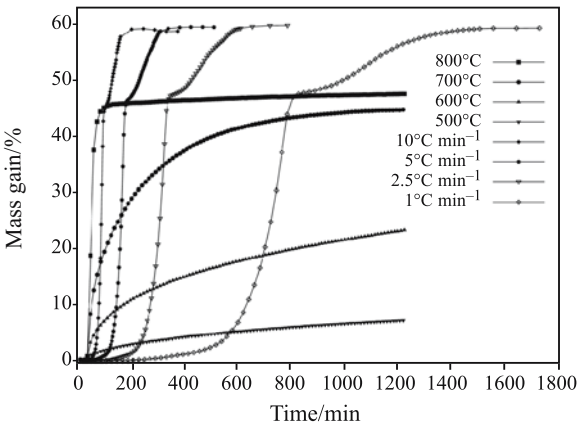

Fig. 6 Non-isothermal TG curves with holding time of 4 h at 1550°C and isothermal TG curves for the oxidation of $ZrSi_2$ powder

Fitting a variety of different consecutive and branching two-step processes, based on either diffusion (D3F, D4, D3), phase boundary (R3, R2) or n-th order reactions (Fn), yielded only a poor description of the experimental TG data. This is demonstrated in Fig. 7, where the best fitting results for a two-step oxidation model according to Eqs (3a) and (3b), based on diffusion reactions of the type D3F are shown. As can be seen from Fig. 7a, the influence of the heating rateon the mass change of the first oxidation step cannot reproduced correctly. The corresponding kinetic parameters are summarised in Table 2.

Therefore, a third step was allowed in the modelling, which introduces an additional degree of freedom. With three-step processes the quality of the fit improved significantly and the complex features of the TG data, in particular the influence of the heating rate on the mass gain of the first oxidation step (Fig. 8a), which is an indication of a branched reaction pathway [7], can be satisfactorily reproduced. The best fitting three-step model consists of two concurrent and one parallel reaction step based on 3D diffusion mechanisms (D3F) and a fractal reaction order (Fn). The underlying differential equations for this model are:

$$\begin{aligned}\frac{da}{dt}&=-A_1\exp\left(-\frac{E_1}{RT}\right)f(a)-A_2\exp\left(-\frac{E_2}{RT}\right)f(a)\\ \frac{db}{dt}&=A_1\exp\left(-\frac{E_1}{RT}\right)f(a)+A_3\exp\left(-\frac{E_3}{RT}\right)f(c)\\ \frac{dc}{dt}&=A_2\exp\left(-\frac{E_2}{RT}\right)f(a)-A_3\exp\left(-\frac{E_3}{RT}\right)f(c)\end{aligned} \qquad (5)$$

where a, b, c are the relative concentrations of the educt, final product and intermediate reaction product, respectively. The D3F diffusion model implemented in the Thermokinetics software is an approximation for the exact solution of Fick's law [15]. The appropriate equations for this reaction type are given in the appendix. The intermediate and final products of this formal multi-step kinetic model are to be viewed as pseudo-components and may comprise different chemical species, but these pseudo-components can be linked with the actually occurring intermediate phases and products formed during the oxidation of $ZrSi_2$. The results from the non-linear regression analysis are summarised in Table 3 and a comparison of measured and calculated degree of reaction is given in Fig. 8. The overall agreement is very good over the entire reaction extent and simultaneously matches the shift in profile location with heating rate as well as the isothermal profiles.

The branching reaction pathway may be explained by the simultaneous occurrence of two oxidation

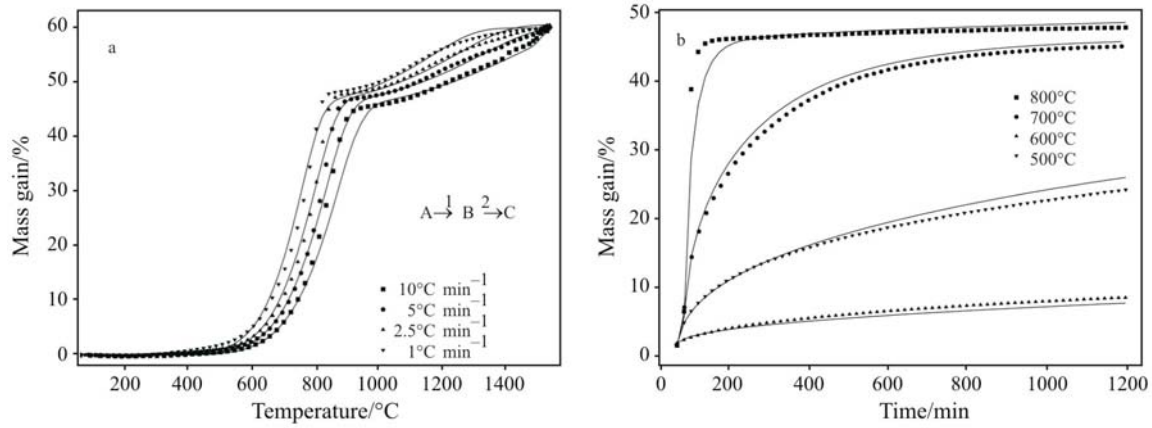

Fig. 7 Comparison of measured and calculated reaction extent for a two-step oxidation model (A→B→C) according to Eqs (3a) and (3b), based on diffusion reactions of the type D3F. (a – constant heating rate data with holding time and b – isothermal data; symbols: measured, lines: calculated)

mechanisms during the first stage of $ZrSi_2$ oxidation, as represented schematically by Eq. (6a) and (6b):

$$ZrSi_2 \xrightarrow{O_2} ZrO_2 + 2Si \quad (6a)$$

$$ZrSi_2 \xrightarrow{O_2} ZrO_2 + 2SiO_2 \quad (6b)$$

Equation (6a) corresponds to the selective oxidation of zirconium in the intermetallic compound. Concurrently to this selective oxidation reaction of zirconium, the more noble constituent, silicon, of the intermetallic compound is already oxidized (Eq. (6b)). Consequently $ZrSi_2$ oxidation proceeds in a not purely selective manner, but as concurring selective and non-selective oxidation mechanisms. The agreement of the results with the branched reaction mechanism consisting of two D3F equations is an indication that the rate controlling step is the diffusion of different chemical species through the growing multiphase oxide layer. In a third step the newly formed Si is oxidized to SiO_2. This third oxidation step occurs at higher temperatures and for complete-oxidation of the $ZrSi_2$ powder particles temperatures up to 1550°C are necessary. An explanation for the observed consistency with a fractal order reaction for the third step cannot be given unambiguously because the physical properties of the multi oxide film change during the last stage of the oxidation reaction. At this stage the phase formation of zircon ($ZrSiO_4$) takes place, which is associated with a change of the diffusion coefficients in the oxide film and it is likely that the oxide film cracks due to mechanical stresses developed during the oxidation reactions, in particular at the higher heating rates.

According to the Xray, TG/DTA and kinetic results, following reaction scheme for the complete oxidation of $ZrSi_2$ particles in flowing air is proposed:

$$ZrSi_2 \xrightarrow[T>500°C]{O_2} ZrO_2 + (2-y)SiO_x + ySi \xrightarrow[T>800°C]{O_2} ZrO_2 + 2SiO_2 \quad (7)$$

whereas the first oxidation step of Eq. (7) is a combination of the two concurrent reactions (6a)

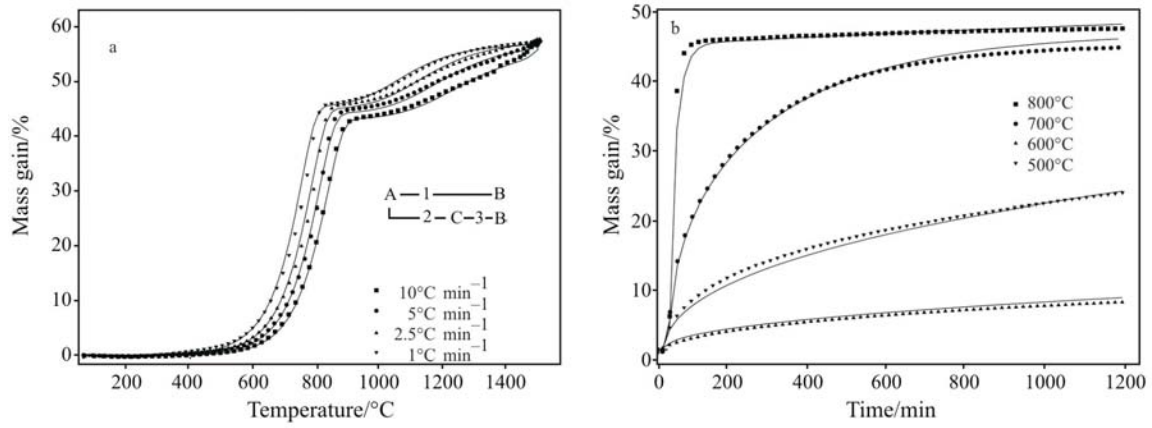

Fig. 8 Comparison of measured and calculated reaction extent for the best fit branching three-step oxidation of $ZrSi_2$ using the parameters in Table 3. Steps 1 and 2 invoke the D3F diffusion equation and step 3 the n^{th} order equation. (a – constant heating rate data with holding time and b – isothermal data; symbols: measured, lines: calculated)

and (6b). Finally, at temperatures of about 1300°C the formation of $ZrSiO_4$ begins to take place and after complete oxidation, the $ZrSi_2$ samples consist of $ZrSiO_4$, amorphous and crystalline SiO_2, as well as some residual ZrO_2. It should be stressed, however, that the determined kinetic parameters, in particular the pre-exponential Arrhenius factor, which is highly dependent on the particle size, are only valid for the investigated experimental conditions such as gas atmosphere, temperature range and powder particle size.

Conclusions

Non-isothermal and isothermal thermogravimetry was used to investigate the heterogeneous gas-solid oxidation of $ZrSi_2$ powder under flowing air up to temperatures of 1550°C. The experimental TG curves clearly suggest a well resolved, multi-step process for the oxidation and therefore a model-fitting kinetic analysis based on multivariate non-linear regression was conducted. The selective oxidation of $ZrSi_2$ results in the formation of elemental Si, ZrO_2 and SiO_x as intermediate oxidation products which are further oxidized with increasing temperature. The complex overall reaction can be best described with a three-step reaction scheme consisting of two branching reactions of the type D3F followed by a fractal order reaction Fn. The two branching reactions can be associated with the simultaneous occurrence of two concurrent oxidation mechanisms. In one reaction pathway $ZrSi_2$ is selectively oxidized to ZrO_2 and Si. The other pathway is described by the non-selective oxidation of $ZrSi_2$ to ZrO_2 and SiO_x. At higher temperatures the selectively formed Si is further oxidized in a third step. The determined kinetic model can be used for process control and optimisation and can be readily incorporated into more complicated source and sink models for real applications like the reaction bonding of zircon-based ceramics or zirconia-alumina-mullite ceramics by the direct oxidation of $ZrAl_3/ZrSi_2$ powder compacts.

Appendix

The approximation formula used in the Thermokinetics software for the exact solution of Fick's law for the three dimensional case (D3F) is:

$$f(\alpha)=4.62755136\begin{cases}\exp(-1.05640725\ln(0.1)) \\ \text{for } \alpha \geq 0.1 \\ \exp(-1.05640725\ln(0.1)) \\ (1-\alpha)/0.9/ \\ [1.0+9.608828(\alpha-0.1)^2- \\ -3.5600323(\alpha-1)^3] \text{ for } \alpha \geq 0.1\end{cases}$$

References

1 H. M. Ondik and H. F. McMurdie, Phase Diagrams for Zirconium + Zirconia Systems, The American Ceramic Society 1998, p. 423.
2 H. Okamato, Bull. Alloy Phase Diagrams, 11 (1990) 513.
3 V. D. Hennige, J. Haußelt, H.-J. Ritzhaupt-Kleissl and T. Windmann, J. Eur. Ceram. Soc., 19 (1999) 2901.
4 N. Claussen, T. Le and S. Wu, J. Eur. Ceram. Soc., 5 (1989) 29.
5 O. Hönigschmid, Monatsh. Chem., 27 (1906) 1069.
6 V. A. Lavrenko, V. Zh. Shemet and A. V. Goncharuk, Thermochim. Acta, 93 (1985) 501.
7 J. Opfermann, Netzsch Thermokinetics 2, Version 2004.05, Netzsch Gerätebau GmbH.
8 H. Geßwein, J. R. Binder, H.-J. Ritzhaupt-Kleissl and J. Haußelt, J. Eur. Ceram. Soc., 26 (2006) 697.
9 J. Opfermann, J. Therm. Anal. Cal., 60 (2000) 641.
10 C. Wagner, J. Electrochem. Soc., 99 (1952) 368.
11 C. Wagner, J. Electrochem. Soc., 103 (1956) 627.
12 C. Wagner, Z. Electrochemie, 63 (1959) 773.
13 H. Geßwein and J. R. Binder, Thermochim. Acta, 444 (2006) 6.
14] J. P. Sanders and P. K. Gallagher, J. Therm. Anal. Cal., 72 (2003) 777.
15 B. Serin and T. Ellickson, J. Chem. Phys., 9 (1941) 742.

Received: March 21, 2007
Accepted: June 12, 2007
OnlineFirst: October 13, 2007

DOI: 10.1007/s10973-007-8461-5